JCI The Journal of Clinical Investigation

Glioma escape signature and clonal development under immune pressure

Cecile L. Maire, … , Manfred Westphal, Katrin Lamszus

J Clin Invest. 2020. https://doi.org/10.1172/JCI138760.

Research In-Press Preview Immunology Oncology

Graphical abstract

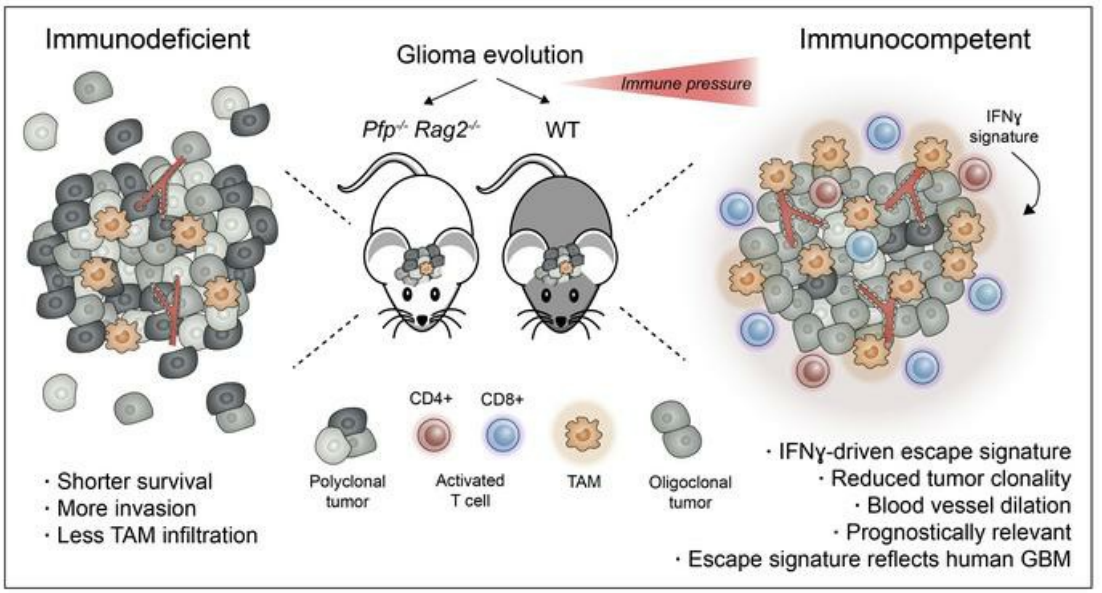

Glioma escape signature and clonal development under immune pressure

Cecile L. Maire[1,9], Malte Mohme[1,9], Michael Bockmayr[2,3], Krystian D. Fita[1], Kristoffer Riecken[4], Daniela Börnigen[5], Malik Alawi[5], Antonio Failla[6], Katharina Kolbe[1], Svenja Zapf[1], Mareike Holz[1], Katrin Neumann[7], Lasse Dührsen[1], Tobias Lange[8], Boris Fehse[4], Manfred Westphal[1], Katrin Lamszus[1]

[1] Department of Neurosurgery, University Medical Center Hamburg-Eppendorf, Hamburg, Germany

[2] Department of Pediatric Hematology and Oncology, University Medical Center Hamburg-Eppendorf, Hamburg, Germany

[3] Charité – Universitätsmedizin Berlin, corporate member of Freie Universität Berlin, Humboldt University Berlin and Berlin Institute of Health, Institute of Pathology, Berlin, Germany

[4] Research Department Cell and Gene Therapy, Department of Stem Cell Transplantation, University Medical Center Hamburg-Eppendorf, Germany

[5] Bioinformatics Core Facility, University Medical Center Hamburg-Eppendorf, Hamburg Germany

[6] UKE Microscopy Imaging Facility, University Medical Center Hamburg-Eppendorf, Germany

[7] Institute of Experimental Immunology and Hepatology, University Medical Center Hamburg-Eppendorf, Hamburg, Germany

[8] Institutes of Anatomy and Experimental Morphology and Pathology, University Cancer Center Hamburg, Hamburg, Germany

[9] These authors contributed equally

Corresponding authors:

Katrin Lamszus, Laboratory for Brain Tumor Biology, Department of Neurosurgery, University Medical Center Hamburg-Eppendorf, Martinistrasse 52, 20246 Hamburg, Germany, lamszus@uke.de, phone +49 40 7410 55577, fax: +49 40 7410 55590

Malte Mohme, Department of Neurosurgery, University Medical Center Hamburg-Eppendorf, Martinistrasse 52, 20246 Hamburg, Germany, m.mohme@uke.de, phone +49 40 7410 56734, fax: +49 40 7410 55590

Conflict of interest: The authors have declared that no conflict of interest exists.

Abstract

Immunotherapeutic strategies are increasingly important in neuro-oncology and the elucidation of escape mechanisms which lead to treatment resistance is crucial. We investigated the impact of immune pressure on the clonal dynamics and immune escape signature by comparing glioma growth in immunocompetent versus immunodeficient mice. Glioma-bearing wildtype and *Pd-1*$^{-/-}$ mice survived significantly longer than immunodeficient *Pfp*$^{-/-}$ *Rag2*$^{-/-}$ mice. While tumors in *Pfp*$^{-/-}$ *Rag2*$^{-/-}$ mice were highly polyclonal, immunoedited tumors in WT and *Pd-1*$^{-/-}$ mice displayed reduced clonality with emergence of immune escape clones. Tumor cells in wildtype mice were distinguished by an interferon-γ-mediated response signature with upregulation of genes involved in immunosuppression. Tumor-infiltrating stromal cells, which include macrophages/microglia, contributed even stronger to the immunosuppressive signature than the actual tumor cells. The identified murine immune escape signature was reflected in human patients and correlated with poor survival. In conclusion, immune pressure profoundly shapes the clonal composition and gene regulation in malignant gliomas.

Introduction

Glioblastoma represents the most frequent aggressive intrinsic brain tumor and patient outcome remains uniformly fatal despite improved treatment options (1). The current era of glioblastoma therapy is being redefined by immunotherapeutic approaches, including immune checkpoint inhibition, oncolytic virus therapy, vaccination strategies and adoptive T cell transfer (2). While the results of several recent clinical trials are encouraging, the effects of immunotherapy have certainly not yet reached their full potential, and the profound tumor-induced immunosuppression and evasion of immune recognition by the tumor cells remains a major challenge for upcoming immunotherapeutic trials (3, 4).

The biology of cancer immune escape, which hinders the execution of efficient immune-mediated cancer elimination, is still incompletely understood. In healthy individuals, cancer cells are recognized and destroyed by the immune system. However, if eradication is unsuccessful, tumor cells can enter an equilibrium phase in which they progressively develop and refine mechanisms to evade immune recognition and elimination, a process conceptualized in the cancer immunoediting hypothesis (5). Initial studies in carcinogen-induced sarcoma models showed that the adaptive immune system and in particular interferon-producing lymphocytes are responsible for preventing tumor outgrowth and maintenance of the equilibrium state (6, 7). Tumors that manage to eventually escape immune control have been selected for phenotypic tumor cell variants invisible to the adaptive tumor-immune response and fit to resist immune attack (6-8). While studies in other cancer types, such as sarcoma or lymphoma pioneered our understanding of such processes, intracranial tumors are remarkably different. They arise in a partially immunoprivileged microenvironment, display a low mutational burden and induce an exceptionally severe T-cell dysfunction with sequestration of T cells in the bone marrow, which does not occur in peripheral tumors (9). It is therefore of particular importance to decipher the mechanisms by which cancer immunoediting shapes the tumor biology in malignant gliomas.

In the present study, we leveraged orthotopic syngeneic immunocompetent and immunodeficient models to gain deeper insight into glioma immune escape mechanisms. We

demonstrate that cancer immunoediting not only shapes the gene expression signature during glioma evolution, but that the selective pressure of the immune system also has a fundamental impact on the clonal composition of tumors arising in the brain. Furthermore, we demonstrate that the identified immune escape signature is relevant in human glioma patients. A better understanding of the mechanisms of how immune escape clones are selected for can support the design of immunotherapeutic strategies that counteract these processes, in order to mount a more effective immune response against immuno-resistant clones.

Results

The immune system impacts glioma survival and alters the tumor morphology

To investigate the impact of the immune system on the growth behavior of intracranial gliomas, we compared the survival and histomorphological characteristics of two syngeneic glioma cell lines in C57BL/6 WT mice and immunodeficient C57BL/6 *Pfp*$^{-/-}$ *Rag2*$^{-/-}$ mice (Figure 1A). The *Pfp*$^{-/-}$ *Rag2*$^{-/-}$ knockout results in complete T- and B-cell deficiency as well as in a severely compromised NK cell function due to the lack of perforin expression. Intracerebral injection of GL261 and CT2A glioma cells in *Pfp*$^{-/-}$ *Rag2*$^{-/-}$ mice resulted in a significantly shorter survival compared to immunocompetent WT mice (median survival GL261: 18 vs. 22 days, $P = 0.012$; CT2A: 14 vs. 20 days, $P = 0.003$), indicating that the functional immune system impairs tumor growth in the brain (Figure 1B, C).

Gliomas in *Pfp*$^{-/-}$ *Rag2*$^{-/-}$ mice grew more invasive and typically also formed large extracerebral masses in addition to the main tumor mass located in the striatum, whereas extracerebral growth was uncommon in WT mice and instead tumors appeared to be more hemorrhagic on macroscopic inspection (Figure 1D). Histological analysis confirmed the increased invasiveness of gliomas in *Pfp*$^{-/-}$ *Rag2*$^{-/-}$ mice (Figure 1E). While GL261 cells tended to infiltrate the brain diffusely, CT2A cells preferentially exhibited a perivascular invasion pattern.

Immunohistochemistry confirmed the absence of infiltrating CD3^{+} T cells (Figure 1F) and B cells (not shown) in *Pfp*$^{-/-}$ *Rag2*$^{-/-}$ mice and showed that the majority of T cells in WT mice were CD8^{+}. Infiltration with Iba1-positive tumor-associated macrophages (TAMs), which can be

either of peripheral origin or represent brain-intrinsic microglia, was strikingly increased in WT mice compared to *Pfp*$^{-/-}$ *Rag2*$^{-/-}$ mice (GL261: mean 11.88% vs. 5.98%, $P = 0.039$; CT2A: mean 35.42% vs. 23.43%, $P = 0.010$), (Figure 1F, G). Intratumoral microvessel densities were not significantly different, however, blood vessels were more dilated in WT mice, possibly due to increased inflammatory signaling (Figure 1F, G). Taken together, these findings suggest that the presence of a functional immune system shapes the growth morphology during glioma evolution in murine brain.

Immuno-editing of the gene expression signature during tumor development

To determine how gene expression is regulated over time by the persistent challenge of an immunocompetent microenvironment, we performed microarray analyses of GL261 tumors at three different timepoints, including days 7 and 14 after injection and the survival endpoint (Figure 2A). Tumors were excised from brains of WT and *Pfp*$^{-/-}$ *Rag2*$^{-/-}$ mice, and tumor RNA from two different mice was pooled for expression profiling. Unsupervised cluster analysis showed that tumor samples separated mainly according to mouse type rather than timepoint (Supplemental Figure 1). The similarity between the expression profiles on day 14 and the endpoint indicates that by day 14 immune escape mechanisms were stably established in WT mice.

In total, 531 genes were overexpressed, and 398 genes were underexpressed $\geq$ 2-fold in WT versus *Pfp*$^{-/-}$ *Rag2*$^{-/-}$ mice (Figure 2B). Gene ontology (GO) and KEGG pathway analysis revealed that genes upregulated on day 7 in tumors in WT mice were most significantly enriched in the term "immune response" and were further strongly enriched in terms related to antigen processing and presentation as well as inflammation (Supplemental Table 1). On day 14, "immune response" continued to be the predominant pathway, but upregulated genes were now increasingly enriched in adaptive immune response pathways, including T- and B-cell activation. Overexpression of immune-related genes was decreased when mice became symptomatic, indicating that once tumors have successfully escaped immune control, high-level expression of immune regulators is no longer essential.

The infiltration of tumors with immune cells followed a similar time course as the regulation of immune-related genes. Infiltration with $CD3^+$ T cells, including $CD8^+$ T cells (Supplemental Figure 2) and macrophages/microglia was maximal on day 14 and decreased when mice became symptomatic (Figure 2C). Concomitantly, expression of PD-L1 in tumors in WT mice was strongest on day 14, while PD-L1 was undetectable in *Pfp*$^{-/-}$ *Rag2*$^{-/-}$ mice at any timepoint. These dynamics were reflected at the transcriptional level, with *Cd3e*, *Cd68* and *Cd274* expression peaking on day 14 in WT mice (Figure 2D). T-cell infiltration was further accompanied by increased expression of co-stimulatory molecules, such as *Cd40 and Cd86,* as well as *Cd74* which is involved in antigen presentation. Moreover, prominent genes associated with immunosuppression beyond *Cd274*, such as *Tgfb1*, *Fas* and *Arg1* displayed similar expression kinetics (Figure 2D). To obtain a more comprehensive picture of immune gene regulation, we further assessed the expression of a set of key immuno-modulators that were identified by Thorsson *et al.* through a meta-analysis of more than 10,000 tumors across 33 diverse cancer types including gliomas (10), as well as the expression time course of cyto- and chemokines (Supplemental Figure 3). Heatmap representation of the immunomodulators contained in our dataset highlighted overexpression of nearly all stimulatory and inhibitory modulators as well as antigen presentation molecules in WT mice, mostly with a peak of expression activity on day 14 (Figure 3). Collectively, these findings indicate that the immune pressure has a maximum effect on adaptive gene regulation around this timepoint which may reflect a critical period in cancer immunoediting, after which the tumor cells have successfully overwhelmed the immune system.

RNA sequencing of isolated tumor cells identifies an immune-escape gene expression signature

While the microarray analysis had revealed that the immune system has a strong dynamic impact on gene regulation in developing tumors over time, this approach had not allowed us to determine what part of the expression signature was derived from the actual glioma cells or from intermixed stromal cells, such as macrophages and microglia which can account for 30–

50% of the tumor mass in malignant gliomas (11). To address this question, we next marked GL261 cells with green fluorescent protein (GFP) and injected them into WT and *Pfp*$^{-/-}$ *Rag2*$^{-/-}$ mice (Figure 4A). Mice were sacrificed when they became symptomatic, and GL261 GFP^{+} tumor cells as well as non-tumor stromal cells were isolated by flow-cytometric cell sorting. Separated cells as well as unsorted bulk tumor samples and in vitro cultured GL261 cells were analyzed by RNA sequencing (RNAseq), (Figure 4A).

Principal component analysis (PCA) showed that tumor cells grown in vivo clustered apart from the in vitro cell line and that sorted GFP^{+} tumor cells separated from bulk tumors, confirming the successful isolation process (Figure 4B). Differences between sorted tumor cells from WT and *Pfp*$^{-/-}$ *Rag2*$^{-/-}$ mice were less pronounced, while the tumor cells clustered widely apart from non-tumor stromal cells in WT mice, underlining the necessity for dissecting the microenvironmental background. Stromal cells from *Pfp*$^{-/-}$ *Rag2*$^{-/-}$ mice could not be analyzed since the RNA yield was too low, presumably due to the significantly reduced TAM infiltration in these mice (Figure 1F, G).

In total, 5172 genes were differentially expressed between purified tumor cells from WT or *Pfp*$^{-/-}$ *Rag2*$^{-/-}$ mice, WT stromal cells or in vitro cultured cells, using a false discovery rate (FDR) < 0.05 and a $\log_2$ fold change (FC) > 2. Unsupervised clustering confirmed the relative similarity between tumor cells in WT and *Pfp*$^{-/-}$ *Rag2*$^{-/-}$ mice and their separation from non-tumor stromal cells (Figure 4C). The majority of genes overexpressed in stromal cells were significantly enriched in pathways associated with immune and inflammatory responses, including adaptive and innate immunity, and in particular T-cell activation (Figure 4D). In contrast, expression signatures of tumor cells in vivo were mainly related to cell cycling and division. To obtain a more detailed view on immune activating as opposed to immunosuppressive responses, we compiled a list of immunosuppressive genes from the literature (4, 12-15) to determine their origin of expression. Interestingly, the vast majority of immunosuppressive cytokines, enzymes, checkpoint ligands and cell surface molecules as well as signaling pathways were overexpressed in the stromal cells rather than in the tumor cells themselves (Figure 5),

indicating that the immunosuppressive signature in gliomas mainly originates from tumor-associated stromal cells, the majority of which consist of macrophages and microglia.

In order to determine how the actual tumor cells adapt to the enduring immune challenge in WT mice and establish mechanisms of immune escape, we excluded the dominant signature of the stromal cells and restricted the analysis to the comparison of tumor cells only. Clustering based on 4148 differentially expressed genes identified 6 main clusters, of which 4 represented transcripts differentially up- or downregulated in the different types of mice (Figure 6A, Supplemental Table 2). Genes upregulated in WT mice were mainly related to an immune response signature, including interferon-γ (IFNγ), interleukin and cytokine signaling pathways (cluster 1, Figure 6B). Querying the Interferome database (www.interferome.org), we found that 57% of the genes overexpressed in cluster 1 are induced by interferons. Network assembly of the regulatory interactions between differentially expressed genes in clusters 1-4 identified interferon regulatory factor 1 (*Irf1*) as a key transcriptional regulator of the interferon-response signature (Figure 7). Upregulated genes linked with this factor include prominent candidates involved in immune escape, such as *Cd274* (PD-L1), *Ctla4*, *Socs1*, *Arg1, Tnfrsf14, Il18bp* as well as in immune stimulation, including *Cxcl9*, *Cxcl10*, *Ciita*, *Ccl6, Ccl8, Ccl24* and *Tnfsf13b* (Figure 7, Supplemental Figure 4). A number of the genes upregulated in tumor cells have been previously associated primarily with TAMs, including *Arg1*, *Cd274*, *Ccl24*, *Ciita*, *Cd74* and other MHC class II pathway-related genes, or with T cells (*Ctla4*, *Il12rb1*), suggesting that tumor cells can in part recapitulate the expression patterns of immune cells when exposed to immunoselective pressure. Collectively, these findings demonstrate that the selective pressure of the immune system shapes the gene expression signature of glioma cells mainly by activating interferon-regulated pathways, which results in upregulation of potent immunosuppressive genes.

Comparisons with human gene expression data highlight the relevance of the immune escape signature

After identifying an immuno-edited gene expression signature in mice, we next assessed its translational relevance in human gliomas. To this end, we analyzed a dataset of 1135 high-grade gliomas that was compiled by Bockmayr *et al.* (16) through a meta-analysis of previously published glioma microarray datasets (17-25). First, we evaluated our finding of a correlative infiltration of tumor tissue with T cells and microglia/macrophages (Figure 2C). In human malignant gliomas the “cytotoxic lymphocyte” and “CD8 T-cell” signatures correlated with the infiltration of “monocytic lineage” cells (both $P < 0.001$), and these correlations were particularly pronounced in IDH-mutated tumors (Figure 8A), supporting our observation that TAM infiltration increases in tumors under immune attack.

Next, we analyzed whether the four differentially regulated gene expression clusters (Figure 6A) are enriched in human T-cell-rich gliomas vs. T-cell depleted gliomas, i.e. the 20% of tumors with the highest expression vs. the 20% of tumors with the lowest T-cell signature (16). Cluster 1 which represents genes overexpressed in tumors under immune attack, was found to be highly enriched in T-cell-rich gliomas, especially in IDH-wildtype tumors ($P < 0.001$, Figure 8B). Conversely, cluster 3, which includes genes downregulated in tumors grown in WT mice, was downregulated in T-cell-rich gliomas ($P < 0.041$, Figure 8B). Our analysis further revealed a strong impact of cluster 1 and 4 on patient survival. Genes from these "immune escape" and "cell cycle" clusters, respectively, that were overexpressed in WT mice (Figure 6B), were associated with a significantly poorer survival (Figure 8C). We then focused on selected genes present in cluster 1 that may contribute to the immune escape of gliomas and analyzed their impact on survival, by comparing the 20% of samples with highest versus lowest expression. As expected, high expression of *Cd274* tended to be associated with a shorter survival ($P = 0.120$). In addition, high expression of *Irf1 (*$P = 0.008$), *Socs1* ($P < 0.001$) and *Tnfrsf14* ($P < 0.001$) was associated with a significantly shorter survival (Figure 8D). Consistent with their function in immune activation, overexpression of *Ccl24* and *Ciita* tended to be associated with prolonged survival. However, some other immune activation genes were

associated with a shorter survival, for example *Cxcl10* and *Ccl8*, suggesting that they may serve additional functions, such as autocrine stimulation of tumor cell growth. Notably, *Apol6* was the second highest overexpressed gene in cluster 1 (330-fold), and this gene which has a largely unknown function, also tended to be associated with a worse prognosis (Supplemental Figures 4, 5), suggesting a potential role in immunosuppression.

The immune environment shapes glioma heterogeneity in vivo

The upregulation of immunosuppressive genes in tumors grown in WT mice is consistent with the concept of cancer immunoediting and the paradigm that during tumor evolution only cells survive that are capable of resisting immune attack. To investigate how the immuno-active environment affects the clonal composition during tumor evolution, we used a multicolor cell tracking system (26, 27). GL261 cells were simultaneously transduced with lentiviral vectors that mediate highly variable expression of random combinations of the three basic colors red-green-blue (RGB), thereby displaying all perceivable colors, comparable to the rainbow spectrum (Figure 9A). RGB-labeled GL261 cells were injected into the brain of WT and *Pfp*$^{-/-}$ *Rag2*$^{-/-}$ mice and tumors were analyzed when mice became symptomatic. Microscopically, tumors in WT mice were composed of fewer different clones than tumors in *Pfp*$^{-/-}$ *Rag2*$^{-/-}$ mice (Figure 9B). To parameterize and quantify this difference, tumors were dissociated, and the clonal composition was analyzed by flow cytometry (Figure 9C). Chromaticity data were represented as 3D plots, and the quantitative analysis of color distributions revealed a significantly higher color contraction in tumors in WT mice compared to *Pfp*$^{-/-}$ *Rag2*$^{-/-}$ mice as well as to the pre-injection cell mix (Figure 9C, D). These findings demonstrate that tumor clonality is reduced in immunocompetent mice, indicating that immune selection pressure restricts the survival and expansion of a number of tumor subclones, while others escape immune control and gain dominance.

Optical barcoding reveals immuno-editing of the clonal architecture

While RGB tracking allows to assess the overall degree of tumor heterogeneity, it is not designed for precise quantification of individual clones due to spectral overlap. To overcome this limitation and assess more precisely how the immune system quantitatively shapes the clonal composition in glioma, we leveraged optical barcoding (OBC) as another technique (28). OBC employs a combinatorial binary approach in which cells are separately transduced with definite combinations of well-distinguishable fluorescent proteins to mark individual clones. By using six different input colors and allowing a maximum of two output colors to be expressed per cell, we generated 21 distinctly color-coded GL261 clones that could stably be re-identified and quantified in mixed populations (Figure 10A).

OBC-labeled GL261 cells were injected into the brain of WT and *Pfp*$^{-/-}$ *Rag2*$^{-/-}$ mice, and we additionally included programmed cell death 1 (*Pdcd1*) knockout (*Pd-1*$^{-/-}$) mice in the experiment as a model of increased immunoselective pressure. Confirming our previous finding (Figure 1B), WT mice survived significantly longer (median 31 days) than *Pfp*$^{-/-}$ *Rag2*$^{-/-}$ mice (median 18.5 days), and *Pd-1*$^{-/-}$ mice survived even longer (median 48 days), suggesting that deficiency of the PD-1 checkpoint further enhances tumor control by the immune system (Figure 10B). To assess the clonal tumor composition, we sacrificed mice when they developed tumor-related symptoms and quantified the OBC-marked tumor cells by flow cytometry. Consistent with the RGB-labeling results, tumors in *Pfp*$^{-/-}$ *Rag2*$^{-/-}$ mice exhibited a highly polyclonal composition with multiple different clones contributing to the tumor mass (Figure 7C-E). In contrast, tumors in WT mice displayed a striking reduction in clonal diversity (mean number of clones > 5% in *Pfp*$^{-/-}$ *Rag2*$^{-/-}$ 4.67 vs. WT 3.05 ($P < 0.001$) and vs. *Pd-1*$^{-/-}$ 3.50 ($P = 0.016$), with predominance of two major clones, GL13 and GL19. Interestingly, in *Pd-1*$^{-/-}$ mice, clones GL13 and GL19 presented the same growth advantage as in the WT mice at earlier timepoints but were later partly eliminated, and instead several other clones successfully escaped immune control and expanded. Repeat experiments confirmed that the clonal diversity was greater in *Pfp*$^{-/-}$ *Rag2*$^{-/-}$ mice than in immunocompetent mice (Figure 10D, Supplemental Figure 6). Moreover, the same two clones were again dominant in tumors in WT

and *Pd-1*$^{-/-}$ mice (Figure 10E), suggesting that they share an extraordinary capacity to escape immune control compared to others. T-cell infiltration in WT tumors was high at day 10 when tumors were still polyclonal, whereas only few T cells remained when mice became symptomatic and when tumor cell heterogeneity was reduced to two major clones (Figure 10F). Since IFNγ secretion by tumor-infiltrating lymphocytes has a major impact on gene regulation in GL261 tumors, and is known to have cytotoxic effects, we analyzed whether IFNγ itself alters the clonal composition in vitro. Incubation of OBC-labeled GL261 cells with IFNγ increased the expression of PD-L1, however, long-term incubation with either 1 or 10 ng/ml IFNγ had only a minor effect on the clonal composition (Supplemental Figure 7A, B). In contrast to our in vivo findings, clone GL13 which was dominant in immunocompetent mice showed a lower prevalence in IFNγ-treated cultures compared to controls. Conversely, clone GL15 which had a relatively high prevalence in tumors in *Pfp*$^{-/-}$ *Rag2*$^{-/-}$ mice expanded relatively more in IFNγ-treated than in untreated cultures. These findings suggest that the presence or absence of IFNγ alone cannot explain the clonal development in mice in vivo and that IFN-induced effects are highly dependent on the tumor microenvironment.

Discussion

While earlier studies on cancer immunoediting primarily focused on carcinogen-induced or spontaneously formed tumors in mice (5), our study investigated the impact of the immune system on tumor development by implanting syngeneic glioma cells into the brain. The major findings of our study are as follows: 1) immunocompetent glioma-bearing mice survive significantly longer than immunodeficient mice; 2) tumors grow more invasive in immunodeficient mice; 3) immune pressure shapes the clonal architecture and profoundly reduces clonal diversity in immunocompetent mice; 4) glioma cells respond to immune selection pressure with activation of interferon response pathways; 5) non-tumor stromal cells are the major origin of the immunosuppressive gene signature in gliomas; 6) the immune

escape signature identified in mice is reflected in human patients and correlates with poor survival.

Our finding that WT mice survived significantly longer than *Pfp*$^{-/-}$ *Rag2*$^{-/-}$ mice indicates that the functional immune system can limit glioma growth in the brain to some extent. Loss of the PD-1 checkpoint conferred an additional survival advantage, consistent with studies in mice and in human glioblastoma patients showing that PD-1 blockade can prolong survival (29, 30). Morphologically, we discovered striking alterations in tumor growth characteristics. Both, GL261 and CT-2A glioma cell lines grew far more invasive in *Pfp*$^{-/-}$ *Rag2*$^{-/-}$ mice, with tumors typically extending also extracerebrally, in contrast to the well-contained intracerebral growth in WT mice. This suggests that local adaptive and innate immune cells may restrict brain invasion in WT mice by tackling glioma cells at the leading edge. In addition, systemic immune control may prevent tumor outgrowth from the relatively protected brain microenvironment into meningeal spaces, supporting the concept of the brain as immunoprivileged site for tumor formation (31).

Our gene expression analysis in bulk tumors over time showed that the majority of genes overexpressed in WT mice were related to an immune response and that differential gene expression compared to *Pfp*$^{-/-}$ *Rag2*$^{-/-}$ mice was maximal on day 14. By the time when mice became symptomatic, downregulation of key immune activators as well as inhibitors had occurred, indicating that the immune response is exhausted and lower levels of endogenous immunosuppressors are required to facilitate tumor progression. T-cell infiltration was also maximal around day 14, consistent with a similar time course described for the T-cell response after infection or vaccination which peaks about 7-15 days after antigen stimulation with a decrease thereafter (32). Tumor infiltration with T cells was further associated with an increased infiltration by macrophages/microglia that was strikingly more pronounced in WT mice than in *Pfp*$^{-/-}$ *Rag2*$^{-/-}$ mice. Accordingly, in human glioma patients “cytotoxic lymphocytes” and “CD8 T cell” signatures correlated with the infiltration by “monocytic lineage" cells, underlining the importance of the interplay between tumor-targeting and immunosuppressive

cell populations, as well as of the continuous stimulatory presence of cytotoxic T cells for the attraction and activation of TAMs.

Macrophages/microglia constitute up to 50% of the cells in human gliomas and thus represent the majority of non-neoplastic cells in the tumors (11). As our bulk tumor analyses had not allowed to determine to what extent the immune response signature was derived from the actual glioma cells as opposed to the non-tumor cells, we injected GFP-marked glioma cells to compare the expression profiles of sorted cell populations. Interestingly the immunosuppressive expression signature mainly originated from the stromal cells. The common perception of immunosuppressive mechanisms in gliomas is that tumor cells secrete cytokines, enzymes, checkpoint ligands and other surface molecules which suppress the adaptive immune response and reprogram macrophages/microglia towards an immunosuppressive M2-like phenotype (4). The reprogrammed TAMs then also contribute to the attenuation of an anti-tumor immune response by expressing additional immunosuppressive factors. Our results demonstrate that the impact of this contribution has likely been underestimated and that TAMs are in fact the major origin of the immunosuppressive expression signature in gliomas. This conclusion is supported by a transgenic model in which microglia depletion resulted in strongly reduced growth of orthotopic GL261 gliomas (33). It remains to be determined whether stromal cell-derived factors are also primarily responsible for the T-cell sequestration in bone marrow that is observed when glioma cells or other cancer cells are implanted into the brain, but not into the subcutaneous microenvironment (9). Our results strongly support the concept that the tumor stroma must be a major target for counteracting immunosuppression in malignant gliomas (11, 34-36).

To determine how immune pressure alters gene regulation in the actual tumor cells and identify mechanisms of the tumor cell-specific immune escape, we specifically compared GFP^+ tumor cells in WT mice versus *Pfp*$^{-/-}$ *Rag2*$^{-/-}$ mice. This comparison revealed that the gene expression signature of immuno-edited glioma cells is dominated by interferon-regulated genes. IFNγ, which is secreted by tumor-infiltrating T cells and NK cells, is known to play a dual role in cancer immunology (37, 38). On the one hand, it is an anti-tumor cytokine that is necessary

for tumor elimination, and IFNγ-deficient mice are more susceptible to tumor formation than WT mice (37, 39). IFNγ causes upregulation of MHC class I on tumor cells, increasing their antigenicity, and it can have anti-proliferative and pro-apoptotic effects on tumor cells (40). Hence, the recent success of neoadjuvant pembrolizumab in recurrent glioblastoma patients was largely attributed to downregulation of cell cycle activity by T cell-derived interferon (29). On the other hand, it was shown for other types of cancer that tumor cells exposed to IFNγ over prolonged times exhibit greater immuno-evasive properties with suppression of cytotoxic T cell and NK cell-mediated immune responses (40). Consistent with this dual role, our study demonstrates that interferon-regulated genes that were overexpressed in gliomas in WT mice include prominent candidates involved in immunosuppression as well as in immune activation. Beyond upregulation of the well-known checkpoint-related genes *Cd274* (9-fold) and Ctla4 (5-fold), we identified *Socs1* (7-fold), *Tnfrsf14* (6-fold), *Il18bp* (5-fold) and *Arg1 (78-fold)* as immunosuppressors overexpressed in glioma cells. SOCS1 (suppressor of cytokine signaling 1) is a potent inhibitor of IFNγ-mediated JAK/STAT signaling that takes part in a negative feedback loop to attenuate cytokine signaling (40). TNFRSF14 (tumor necrosis factor receptor superfamily member 14), also known as herpes virus entry mediator (HVEM), is a surface molecule with checkpoint function that was recently discovered to be overexpressed and associated with a poor prognosis in glioblastoma patients (41). IL18bp (interleukin-18 binding protein) is an inhibitor of the proinflammatory cytokine IL-18 that inhibits IL-18-induced IFNγ production (42). *Arg1* encodes the enzyme arginase which is known as a marker of pro-tumorigenic (M2-polarized) macrophages/microglia in gliomas (43) and has not yet been reported to be expressed by tumor cells at significant levels. Arginase depletes L-arginine in the local tumor environment, resulting in the inhibition of T- and NK-cell activation (44). By upregulating *Arg1*, glioma cells thus recapitulate an immunosuppressive mechanism employed by TAMs, similar as has been described for PD-L1 (CD274) (45). Of note, the second highest overexpressed gene in WT tumors was *Apol6* (330-fold). Little is known about the function of this cytoplasmic protein. It is known to be induced by interferon and its expression in HIV-infected T cells can limit the production of infectious virus, suggesting a potential involvement

in immunoregulatory processes (46). High expression of *Apol6* in human glioma patients is associated with shorter survival, supporting the idea that it may contribute to immunosuppression and mandating future studies to address this question.

The fact that the immune escape signature which we identified in murine gliomas is specifically enriched in human T-cell-rich gliomas and is associated with a significantly shorter patient survival highlights the translational relevance of our findings. The comparison with human expression data is particularly important since our models do not recapitulate spontaneous glioma formation in mice which might be associated with different immune responses. A number of genes that are part of the identified murine escape signature have a known immunosuppressive function and are associated with a worse overall patient survival (*Socs1*, *Irf1*, *Tnfrsf14* and *Cd274*). Conversely, several immune-activating genes tend to be associated with a better survival (*Ccl24, Ciita*). However, there are exceptions to this scheme, for example, high expression of the activating chemokine genes *Cxcl10* and *Ccl8* is associated with a worse prognosis while *Il18bp* expression is linked with a better prognosis (not shown). These seemingly paradoxic results indicate that these immune modulators most likely have additional functions in glioma biology and may for example also exert autocrine effects on tumor cell growth or vascular cells by which they promote glioma growth.

In addition to identifying an immune escape signature, our study demonstrates that immune selection pressure profoundly affects tumor heterogeneity and sculpts the clonal tumor architecture. Tumors in *Pfp*$^{-/-}$ *Rag2*$^{-/-}$ mice exhibited a highly polyclonal composition, whereas immuno-edited tumors in WT and *Pd-1*$^{-/-}$ mice displayed greatly reduced clonal diversity, indicating that immunoselective pressure restricts the survival and expansion of certain tumor subclones in WT mice while selecting for escape clones that are capable of resisting immune attack. These findings demonstrate that the local microenvironment, even in a partially immunoprivileged organ such as the brain, is capable of controlling clonal evolution. In multiple repeat experiments we found that always the same two clones (GL13, GL19) became dominant in WT mice. In vitro, these clones did not have a growth advantage over others, and in *Pfp*$^{-/-}$ *Rag2*$^{-/-}$ mice they were outgrown by yet different clones, highlighting the importance of

the individual microenvironment in shaping the clonal composition. Since gene expression profiles of tumor cells in WT mice were mainly distinguished by an interferon-response signature and IFNγ can have cytotoxic effects on cells, we hypothesized that IFNγ by itself may exert clonal selection pressure. However, long-term incubation with IFNγ in vitro had little effect on the clonal composition of GL261 cultures, indicating that the complex in vivo microenvironment with its multilateral interactions between IFNγ-secreting T cells, TAMs, tumor cells and other cells is necessary to achieve the particular selection of immune escape clones that we observed.

Studies in other types of cancer, such as non-small cell lung cancer (NSCLC) or melanoma, showed that neoantigen load is a major factor determining an efficient immune response against tumors (47). In NSCLC patients, high clonal mutational burden and low subclonal mutational heterogeneity correlate with a superior prognosis, and these patients also respond better to immune checkpoint blockade (48). Local mutational burden is associated with local T-cell clonal expansion, suggesting that tumor-immune cell interactions impose negative selection by pruning out tumor cell populations carrying neo-epitopes (49). GL261 cells are hypermutated and the majority of non-synonymous mutations is subclonal (50, 51). It is therefore possible that the two dominant clones in WT mice might display a lower mutational burden and reduced neo-antigenicity in comparison to other clones. In addition, the nature of presented tumor antigens determines the extent of T-cell recognition and activation, and a higher "antigen fitness" may have resulted in depletion of more immunogenic clones during tumor evolution (52). Heterogeneous expression of co-stimulatory or inhibitory ligands, the ability to recruit immunoregulatory cells, or other differences in tumor-immune cell interaction may have added to differences in immunogenicity between individual clones. Further studies are necessary to elucidate the precise mechanisms by which certain clones escape immune control while others become eliminated. To this end, tumor cell clones need to be captured and analyzed at early time points from nascent tumors when immunosensitive clones have not yet been eliminated and can be directly compared to those that later gain dominance.

In conclusion, our study demonstrates that glioma immunoediting is not only defined by alterations in gene expression profiles and growth patterns, but also by distinct clonal selection that reduces tumor heterogeneity. The here identified mechanisms of immune escape can inform translational studies aiming to target tumor-induced immunosuppression, in order to advance the efficacy of tumor-specific immune activation in glioma patients.

Methods

Cell culture

GL261 and CT2A murine malignant glioma cell lines (kindly provided by Dr. Darrell Bigner and Dr. Matthias Gromeier, Duke University, Durham, NC), as well as 293T cells (ATCC CRL-3216) used for production of lentiviral particles were propagated in DMEM containing 4.5 g/L glucose, 4 mM L-Glutamine, and 1 mM pyruvate (31966-021, Gibco), supplemented with 10% fetal bovine serum, 25 mM HEPES, 100 U/mL, penicillin, and 100 mg/mL streptomycin.

Optical barcoding and RGB labeling

Fluorescent optical barcoding (OBC) was performed as described previously (28). Briefly, cells were plated in a 24-well plate at a density of 50,000 cells/well in 500 µl medium. Cells were transduced with lentiviral gene ontology (LeGO) vectors expressing 6 different fluorescent proteins, allowing a maximum of 2 colors per well. Transduced cultures were single-cell sorted into separate wells in a 96-well plate using a BD FACSAria IIIu cell sorter. Clones grown from single cells were re-analyzed and expanded separately. Red-, green- and blue (RGB) marking was performed as described before (26, 27). Cells were transduced simultaneously with equal amounts of three LeGO vectors (LeGO-C2-Puro+, LeGO-V2-Puro+ and LeGO-Cer2-Puro+; www.LentiGO-Vectors.de), each expressing one fluorescent protein. After the optimal MOI was defined (to obtain about 50% to 70% transduction rate per color), cells were selected with 1 µg/mL puromycin and expanded for experiments. The clonal composition of tumors generated in vivo from OBC- or RGB-marked cells was analyzed by flow cytometry (BD LSRFortessa). RGB marking FACS data were visualized and quantified for clonal composition

using an in-house MATLAB-based program adapted from Wu *et al. (53)*. Datasets were filtered based on viability, fluorescence intensities and normalized to in vitro controls. 3D spherical scatter plots were created by normalizing all data point vectors to a length of 1. Chromaticity values were calculated by assigning a radius to all data points and selecting all points on a spherical theta-phi grid within this distance to any data point. Areas between all grid points were calculated and compared to the total surface area of the plot.

Orthotopic in vivo models

GL261 or CT2A cells (1 x 10^5 cells/µl in 2 µl DMEM) were injected into 8-14-week-old female C57BL/6 WT mice (Charles River), C57BL/6 *Pfp*$^{-/-}$ *Rag2*$^{-/-}$ mice (B6.129S6-*Rag2*^{tm1Fwa}*Prf1*^{tm1Clrk} N12, Taconic) or C57BL/6 *Pd-1*$^{-/-}$ mice [B6.Cg-Pdcd1$^{tm1.1Shr}$/J, kindly provided by Dr. Tasuku Honjo, Kyoto University, Kyoto, Japan (54)］as described previously (28). In experiments with OBC-labeled cells, clones were mixed in equal proportions to a final cell concentration of 1 x 10^5 cells/µl and were injected into the right striatum. Animals were euthanized when they developed tumor-related symptoms and brains were either formalin-fixed and paraffin-embedded (FFPE), or tumors were removed, dissociated and processed for flow cytometry.

Microarray analysis

GL261 cells were injected into WT C57BL/6 or *Pfp*$^{-/-}$ *Rag2*$^{-/-}$ mice and tumors were collected on day 7 (n = 4 per mouse type) or day 14 (n = 4 per type) or when mice became symptomatic (n = 6 per type). RNA was extracted from tumor tissue using Nucleospin columns (Macherey Nagel), pooled from 2 or 3 mice and analyzed on Illumina microarray mouse WG-6 v2.0 chips. Raw data were preprocessed using Genepattern from the Broad Institute and with cubic spline normalization (55, 56).

RNA sequencing

Tumors were excised from symptomatic mice (C57BL/6 WT or *Pfp*$^{-/-}$ *Rag2*$^{-/-}$, 6 mice each) previously injected with GL261 GFP$^+$ cells. Single cell suspensions were obtained by

collagenase digestion (1.5 mg/mL, Biochrom). After filtration and washing, the cells were sorted using a BD FACSAria IIIu cell sorter into GFP^+ tumor cells and GFP^- non-tumor cells. These samples were compared to bulk unsorted cells that contained both populations and to GL261 in vitro cultured cells used for mice injection (all in triplicate). RNA was extracted using Nucelospin columns and quantified by the Agilent Bioanalyser RNA 6000 kit. All samples were sequenced in the genomic core facility of Münster University on a NextSeq 500 v2 sequencer, using the NEBNext mRNA isolation module and NEBNext RNA Ultra directional library prep kit. Sequencing reads were aligned to the mouse reference assembly (GRCm38.87) using STAR version 2.5.2b (https://github.com/alexdobin/STAR/releases). Differential expression analysis was carried out using DESeq2 (https://bioconductor.org/packages/release/bioc/html/DESeq2.html) (57). Genes were considered differentially expressed if the FDR was below 0.05 and the $\log_2$FC was above 2.

Immunohistochemistry

Immunohistochemistry was performed on FFPE tissue using a Ventana BenchMark XT stainer (Roche) and the UtlraView DAB detection kit (Roche). The following primary antibodies were used: IBA1 (Wako, 019-19741); CD3 (Abcam, ab 16669); CD8a (Synaptic Systems, 361003); PD-L1 (Lola 6H6, kindly provided by Dr. Thomas Jacobs, Bernhard-Nocht-Institut für Tropenmedizin, Hamburg, Germany); CD34 (Abcam, ab 8158). Blood vessel density was determined by counting the number of CD34 immunoreactive blood vessels in 5 high-power fields (0.031 mm^2 each) in the most densely vascularized tumor hotspot area.

Statistics

Comparison of human and murine data was performed with the statistical programming language R (www.r-project.org), using the packages *survival*, *gplots* and *biomaRt.* Processed gene expression and clinical data of 1135 high-grade gliomas (WHO grade III-IV) as well as signatures of 10 immune and stromal cell populations was obtained from Bockmayr *et al. (16)*. Pearson's correlation coefficient was used for correlation of human immune-stromal

signatures. Significance of correlation was assessed using the R-function *cor.test*. Matching of human and mouse genes was performed with *biomaRt* using the Ensembl gene annotation. T-cell rich/depleted tumors were defined as the 20% tumors with highest/lowest expression of the signature “T cells” (16).

Other statistical tests were applied as indicated in the figure legends. Statistical analyses were performed using GraphPad Prism and IBM SPSS v22. All t-tests were unpaired and two-tailed. Tests for multiple comparisons were performed using the one-way ANOVA with Tukey´s post-hoc test. *P* values < 0.05 were considered significant. Plots were graphed using GraphPad Prism, R Foundation's R v2.12 and Adobe Illustrator CC 2017.

Databases

Murine gene expression profiles were investigated using publicly available databases. Functional annotation and identification of overrepresented GO terms and KEGG pathways were performed using the DAVID 6.7 database (https://david-d.ncifcrf.gov/summary.jsp) (58). Network analysis was performed using Cytoscape version 3.7.1. (https://github.com/cytoscape/cytoscape/releases/3.7.1/) (59). Protein Ensembl identifiers were used to build the network using the STRING database version 11.0 (https://string-db.org/) (60). Genes involved in the interferon gamma regulation and pathways were extracted from the Interferome database (www.interferome.org) (61). Gene expression profiles from murine experiments have been submitted to the GEO database with accession number GSE151285 (https://www.ncbi.nlm.nih.gov/geo/). Human microarray gene expression datasets are publicly available at Cbioportal (http:// www.cbioportal.org/) (62) under the following accession numbers: GSE83130, GSE108474, GSE50161, GSE13041, GSE16011, GSE36245, GSE73038, GSE19578 and GSE26576. Additional information can be found in the publication by Bockmayr *et al.* (16).

Study approval

All animal experiments were performed in accordance with the guidelines of animal welfare and permission of the authority for health and consumer protection in Hamburg.

Author contributions

CM and MM performed the experiments, collected and analyzed the data and prepared the manuscript. MB performed the in silico analysis of published gene expression profiles and prepared the manuscript. KDF analyzed the RNA gene expression data and applied and adapted the bioinformatic tool to quantify RGB heterogeneity experiments. KR and BF generated RGB and OBC labeling constructs, labeled the cell lines and helped with the manuscript. DB and MA performed the bioinformatic analysis. AF helped perform the microscopic analysis of OBC-labeled cells. KK, SZ and MH provided technical support, prepared cell lines and assisted in every aspect of the performed experiments. KN and TL provided additional mouse strains. LD assisted in the mouse experiments and interpreted the human datasets. MW supervised the studies, provided scientific input and critically revised the manuscript. KL supervised the study, analyzed the data and prepared the manuscript.

Acknowledgements

We thank the FACS core facility and the Mouse Pathology Core Facility at the University Medical Center Hamburg-Eppendorf for their excellent support. We are grateful to Dr. Darell D. Bigner and Dr. Matthias Gromeier (Duke University) for providing the GL261 and CT2A cell lines. We thank Anika Witten, Institute for human genetics, University Medical Center Münster, for the excellent support with the RNA sequencing. This study was supported by grants from the Anni Hofmann Stiftung (KL), the Else Kröner-Fresenius-Stiftung (MM), the Johannes-Bauer Stiftung (MW) and the Deutsche Forschungsgemeinschaft (KR, SFB841).

References

1. Westphal M, and Lamszus K. The neurobiology of gliomas: from cell biology to the development of therapeutic approaches. *Nat Rev Neurosci.* 2011;12(9):495-508.
2. Lim M, Xia Y, Bettegowda C, and Weller M. Current state of immunotherapy for glioblastoma. *Nat Rev Clin Oncol.* 2018;15(7):422-42.
3. Mohme M, Neidert MC, Regli L, Weller M, and Martin R. Immunological challenges for peptide-based immunotherapy in glioblastoma. *Cancer Treat Rev.* 2014;40(2):248-58.
4. Mangani D, Weller M, and Roth P. The network of immunosuppressive pathways in glioblastoma. *Biochem Pharmacol.* 2017;130:1-9.
5. Dunn GP, Old LJ, and Schreiber RD. The three Es of cancer immunoediting. *Annu Rev Immunol.* 2004;22:329-60.
6. Koebel CM et al. Adaptive immunity maintains occult cancer in an equilibrium state. *Nature.* 2007;450(7171):903-7.
7. Shankaran V et al. IFNgamma and lymphocytes prevent primary tumour development and shape tumour immunogenicity. *Nature.* 2001;410(6832):1107-11.
8. Matsushita H et al. Cancer exome analysis reveals a T-cell-dependent mechanism of cancer immunoediting. *Nature.* 2012;482(7385):400-4.
9. Chongsathidkiet P et al. Sequestration of T cells in bone marrow in the setting of glioblastoma and other intracranial tumors. *Nat Med.* 2018;24(9):1459-68.
10. Thorsson V et al. The Immune Landscape of Cancer. *Immunity.* 2018;48(4):812-30 e14.
11. Hambardzumyan D, Gutmann DH, and Kettenmann H. The role of microglia and macrophages in glioma maintenance and progression. *Nat Neurosci.* 2016;19(1):20-7.
12. Doucette T et al. Immune heterogeneity of glioblastoma subtypes: extrapolation from the cancer genome atlas. *Cancer Immunol Res.* 2013;1(2):112-22.
13. Platten M, Ochs K, Lemke D, Opitz C, and Wick W. Microenvironmental clues for glioma immunotherapy. *Curr Neurol Neurosci Rep.* 2014;14(4):440.

14. Nduom EK, Weller M, and Heimberger AB. Immunosuppressive mechanisms in glioblastoma. *Neuro Oncol.* 2015;17 Suppl 7:vii9-vii14.

15. Grauer OM, Wesseling P, and Adema GJ. Immunotherapy of diffuse gliomas: biological background, current status and future developments. *Brain Pathol.* 2009;19(4):674-93.

16. Bockmayr M et al. Immunologic Profiling of Mutational and Transcriptional Subgroups in Pediatric and Adult High-Grade Gliomas. *Cancer Immunol Res.* 2019;7(9):1401-11.

17. Ceccarelli M et al. Molecular Profiling Reveals Biologically Discrete Subsets and Pathways of Progression in Diffuse Glioma. *Cell.* 2016;164(3):550-63.

18. Madhavan S, Zenklusen JC, Kotliarov Y, Sahni H, Fine HA, and Buetow K. Rembrandt: helping personalized medicine become a reality through integrative translational research. *Mol Cancer Res.* 2009;7(2):157-67.

19. Griesinger AM et al. Characterization of distinct immunophenotypes across pediatric brain tumor types. *J Immunol.* 2013;191(9):4880-8.

20. Lee Y et al. Gene expression analysis of glioblastomas identifies the major molecular basis for the prognostic benefit of younger age. *BMC Med Genomics.* 2008;1:52.

21. Gravendeel LA et al. Intrinsic gene expression profiles of gliomas are a better predictor of survival than histology. *Cancer Res.* 2009;69(23):9065-72.

22. Sturm D et al. Hotspot mutations in H3F3A and IDH1 define distinct epigenetic and biological subgroups of glioblastoma. *Cancer Cell.* 2012;22(4):425-37.

23. Sturm D et al. New Brain Tumor Entities Emerge from Molecular Classification of CNS-PNETs. *Cell.* 2016;164(5):1060-72.

24. Paugh BS et al. Integrated molecular genetic profiling of pediatric high-grade gliomas reveals key differences with the adult disease. *J Clin Oncol.* 2010;28(18):3061-8.

25. Paugh BS et al. Genome-wide analyses identify recurrent amplifications of receptor tyrosine kinases and cell-cycle regulatory genes in diffuse intrinsic pontine glioma. *J Clin Oncol.* 2011;29(30):3999-4006.

26. Weber K et al. RGB marking facilitates multicolor clonal cell tracking. *Nat Med.* 2011;17(4):504-9.

27. Weber K, Thomaschewski M, Benten D, and Fehse B. RGB marking with lentiviral vectors for multicolor clonal cell tracking. *Nat Protoc.* 2012;7(5):839-49.

28. Mohme M et al. Optical Barcoding for Single-Clone Tracking to Study Tumor Heterogeneity. *Mol Ther.* 2017;25(3):621-33.

29. Cloughesy TF et al. Neoadjuvant anti-PD-1 immunotherapy promotes a survival benefit with intratumoral and systemic immune responses in recurrent glioblastoma. *Nat Med.* 2019;25(3):477-86.

30. Reardon DA et al. Glioblastoma Eradication Following Immune Checkpoint Blockade in an Orthotopic, Immunocompetent Model. *Cancer Immunol Res.* 2016;4(2):124-35.

31. Mrass P, and Weninger W. Immune cell migration as a means to control immune privilege: lessons from the CNS and tumors. *Immunol Rev.* 2006;213:195-212.

32. Pennock ND, White JT, Cross EW, Cheney EE, Tamburini BA, and Kedl RM. T cell responses: naive to memory and everything in between. *Adv Physiol Educ.* 2013;37(4):273-83.

33. Markovic DS et al. Gliomas induce and exploit microglial MT1-MMP expression for tumor expansion. *Proc Natl Acad Sci U S A.* 2009;106(30):12530-5.

34. Szulzewsky F et al. Human glioblastoma-associated microglia/monocytes express a distinct RNA profile compared to human control and murine samples. *Glia.* 2016;64(8):1416-36.

35. Roesch S, Rapp C, Dettling S, and Herold-Mende C. When Immune Cells Turn Bad-Tumor-Associated Microglia/Macrophages in Glioma. *Int J Mol Sci.* 2018;19(2).

36. Glass R, and Synowitz M. CNS macrophages and peripheral myeloid cells in brain tumours. *Acta Neuropathol.* 2014;128(3):347-62.

37. Dunn GP, Koebel CM, and Schreiber RD. Interferons, immunity and cancer immunoediting. *Nat Rev Immunol.* 2006;6(11):836-48.

38. Zaidi MR, and Merlino G. The two faces of interferon-gamma in cancer. *Clin Cancer Res.* 2011;17(19):6118-24.

39. Benci JL et al. Tumor Interferon Signaling Regulates a Multigenic Resistance Program to Immune Checkpoint Blockade. *Cell.* 2016;167(6):1540-54 e12.

40. Zaidi MR. The Interferon-Gamma Paradox in Cancer. *J Interferon Cytokine Res.* 2019;39(1):30-8.

41. Han MZ et al. Immune checkpoint molecule herpes virus entry mediator is overexpressed and associated with poor prognosis in human glioblastoma. *EBioMedicine.* 2019;43:159-70.

42. Dinarello CA. Novel targets for interleukin 18 binding protein. *Ann Rheum Dis.* 2001;60 Suppl 3:iii18-24.

43. Zhang I et al. Characterization of Arginase Expression in Glioma-Associated Microglia and Macrophages. *PLoS One.* 2016;11(12):e0165118.

44. Rodriguez PC et al. Arginase I production in the tumor microenvironment by mature myeloid cells inhibits T-cell receptor expression and antigen-specific T-cell responses. *Cancer Res.* 2004;64(16):5839-49.

45. Berghoff AS et al. Programmed death ligand 1 expression and tumor-infiltrating lymphocytes in glioblastoma. *Neuro Oncol.* 2015;17(8):1064-75.

46. McLaren PJ et al. Identification of potential HIV restriction factors by combining evolutionary genomic signatures with functional analyses. *Retrovirology.* 2015;12:41.

47. Schumacher TN, and Schreiber RD. Neoantigens in cancer immunotherapy. *Science.* 2015;348(6230):69-74.

48. McGranahan N et al. Clonal neoantigens elicit T cell immunoreactivity and sensitivity to immune checkpoint blockade. *Science.* 2016;351(6280):1463-9.

49. Jia Q et al. Local mutational diversity drives intratumoral immune heterogeneity in non-small cell lung cancer. *Nat Commun.* 2018;9(1):5361.

50. Aslan K et al. Heterogeneity of response to immune checkpoint blockade in hypermutated experimental gliomas. *Nat Commun.* 2020;11(1):931.

51. Johanns TM et al. Endogenous Neoantigen-Specific CD8 T Cells Identified in Two Glioblastoma Models Using a Cancer Immunogenomics Approach. *Cancer Immunol Res.* 2016;4(12):1007-15.

52. Luksza M et al. A neoantigen fitness model predicts tumour response to checkpoint blockade immunotherapy. *Nature.* 2017;551(7681):517-20.

53. Wu JW, Turcotte R, Alt C, Runnels JM, Tsao H, and Lin CP. Defining Clonal Color in Fluorescent Multi-Clonal Tracking. *Sci Rep.* 2016;6:24303.

54. Nishimura H, Nose M, Hiai H, Minato N, and Honjo T. Development of lupus-like autoimmune diseases by disruption of the PD-1 gene encoding an ITIM motif-carrying immunoreceptor. *Immunity.* 1999;11(2):141-51.

55. Workman C et al. A new non-linear normalization method for reducing variability in DNA microarray experiments. *Genome Biol.* 2002;3(9):research0048.

56. Reich M, Liefeld T, Gould J, Lerner J, Tamayo P, and Mesirov JP. GenePattern 2.0. *Nat Genet.* 2006;38(5):500-1.

57. Love MI, Huber W, and Anders S. Moderated estimation of fold change and dispersion for RNA-seq data with DESeq2. *Genome Biol.* 2014;15(12):550.

58. Huang da W, Sherman BT, and Lempicki RA. Systematic and integrative analysis of large gene lists using DAVID bioinformatics resources. *Nat Protoc.* 2009;4(1):44-57.

59. Shannon P et al. Cytoscape: a software environment for integrated models of biomolecular interaction networks. *Genome Res.* 2003;13(11):2498-504.

60. Szklarczyk D et al. STRING v11: protein-protein association networks with increased coverage, supporting functional discovery in genome-wide experimental datasets. *Nucleic Acids Res.* 2019;47(D1):D607-D13.

61. Rusinova I et al. Interferome v2.0: an updated database of annotated interferon-regulated genes. *Nucleic Acids Res.* 2013;41(Database issue):D1040-6.

62. Cerami E et al. The cBio cancer genomics portal: an open platform for exploring multidimensional cancer genomics data. *Cancer Discov.* 2012;2(5):401-4.

Figure 1

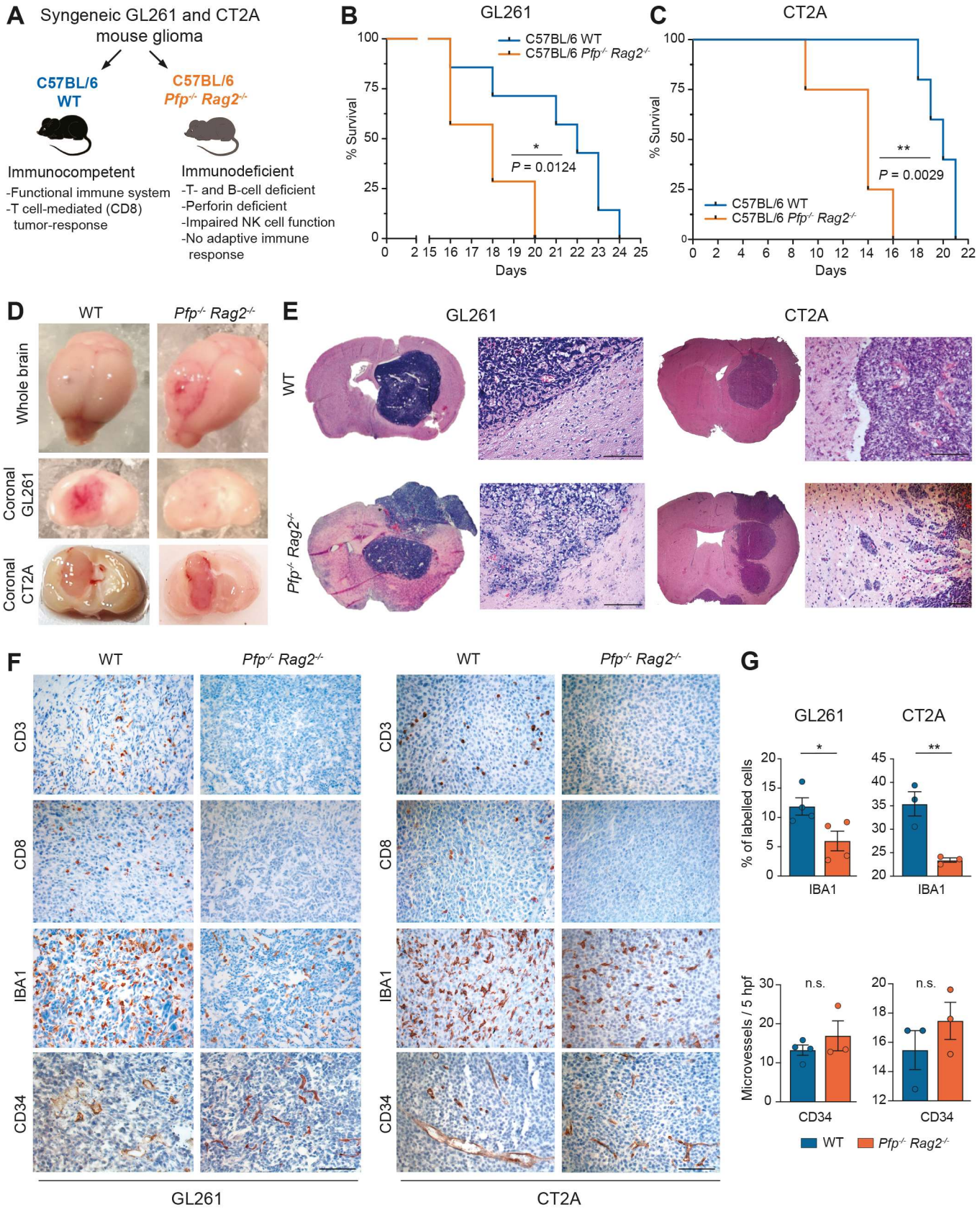

Figure 1: Glioma growth in immunocompetent versus immunodeficient mice.
(**A**) Schematic overview of the experimental setup. (**B**) Kaplan-Meier survival analysis of WT and *Pfp*$^{-/-}$ *Rag2*$^{-/-}$ mice injected intracerebrally with GL261 cells (n = 7/group), log-rank test (**C**) Survival analysis of mice injected with CT2A cells (n = 5 WT, 4 *Pfp*$^{-/-}$ *Rag2*$^{-/-}$). (**D**) Macroscopic tumor appearance. (**E**) H&E staining of tumor sections. (**F**) Immunohistochemistry for CD3, CD8, Iba1 and CD34. (**G**) Quantification of macrophages/microglia (Iba1) and tumor microvessels (CD34). Bars represent means ± SEM; unpaired two-tailed Student´s t-test, for GL261 *P = 0.04, n = 4 and for CT2A **P = 0.01, n = 3; n.s., not significant. Size bars are 100 µm; hpf, high power fields.

Figure 2

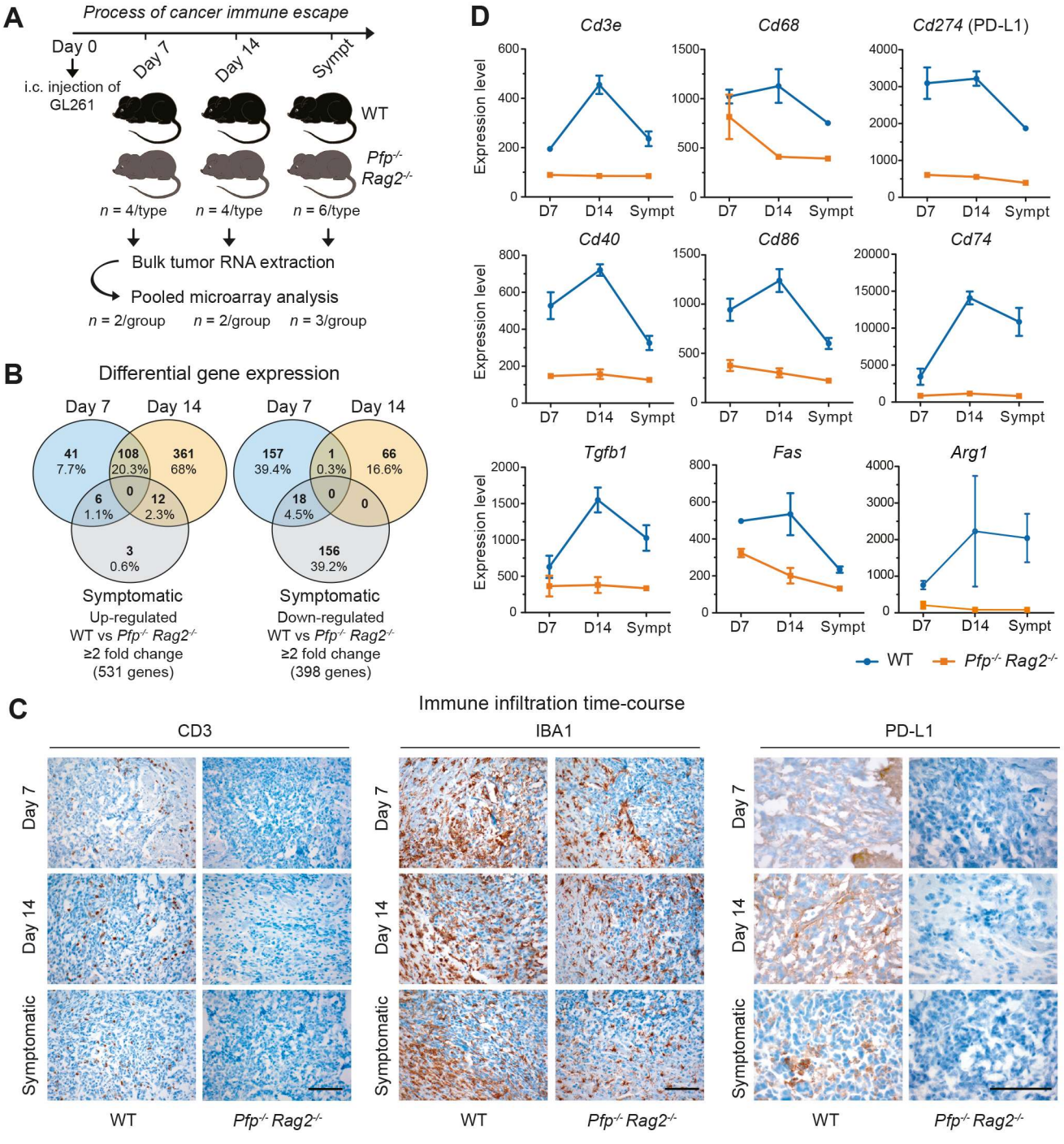

Figure 2: Gene regulation during tumor evolution.
(**A**) Workflow of GL261 tumor analysis. RNA from 2x 2 mice per type (days 7 and 14) or 3x 2 mice per type [symptomatic endpoint (sympt)] was pooled for expression profiling by Illumina WG-6 v2.0 arrays. (**B**) Venn diagrams of genes over- and under-expressed in WT vs. *Pfp*$^{-/-}$ *Rag2*$^{-/-}$ mice. (**C**) Immunohistochemistry for CD3, IBA1 and PD-L1. Size bars are 100 µm. (**D**) Expression values of selected immune-related genes over time. Data are presented as mean ± SEM, day 7 n = 2, day 14 n = 2, symptomatic n = 3.

Figure 3

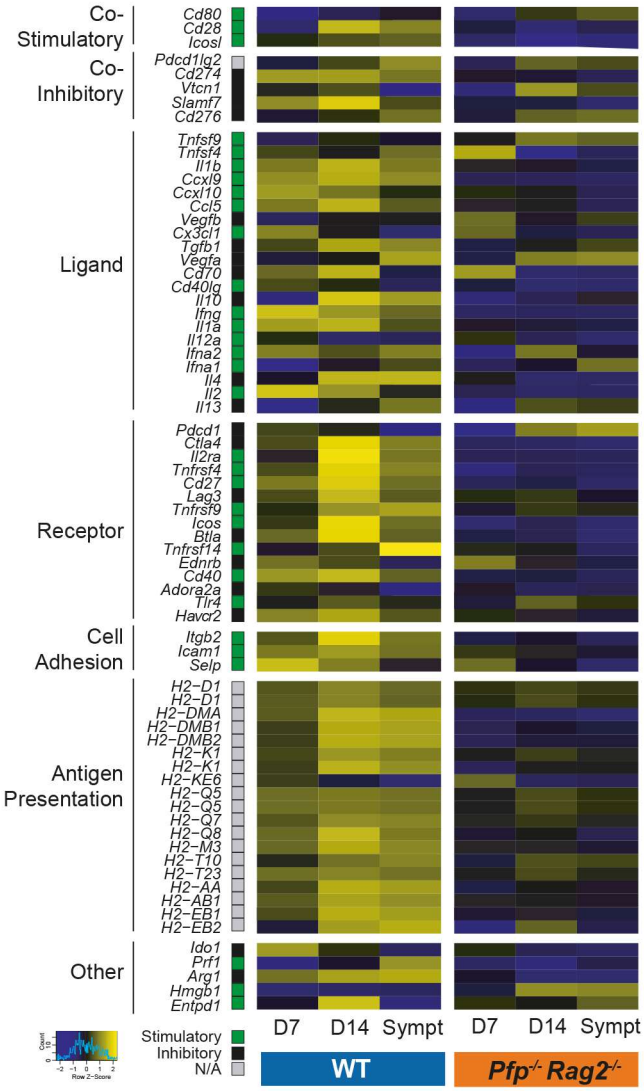

Figure 3: Regulation of immune modulators. Gene expression of stimulatory and inhibitory immune modulators identified by Thorsson *et al.* (10) in our dataset (N/A, not applicable).

Figure 4

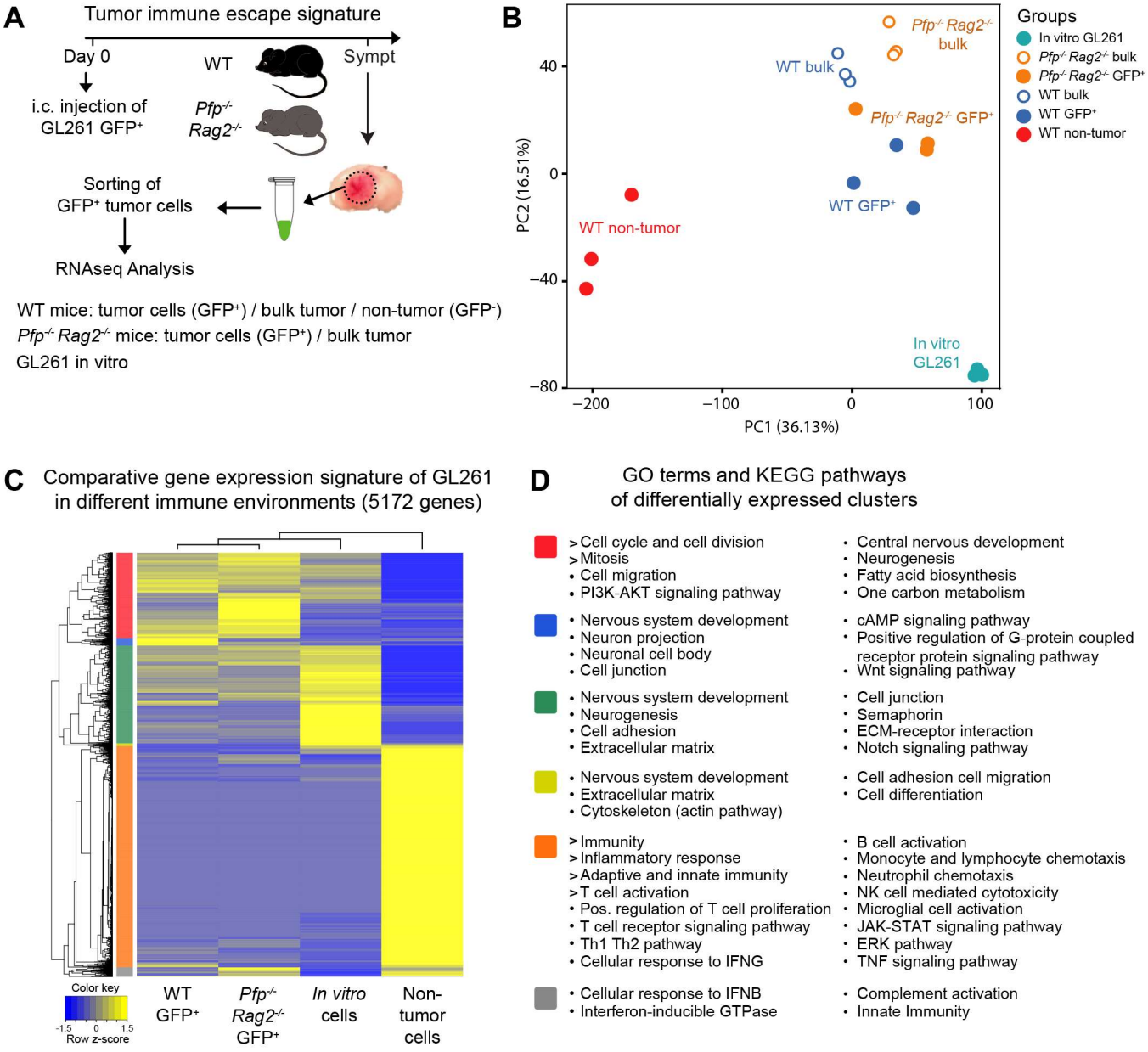

Figure 4: Expression signatures in tumor and non-tumor cell populations.
(**A**) Schematic workflow of GFP-marked GL261 cell injection, flow-cytometric sorting and RNAseq analysis. Stromal cells from *Pfp*$^{-/-}$ *Rag2*$^{-/-}$ mice could not be analyzed due to very low RNA yield from the sparse non-tumor population (see Figure 1E). (**B**) Principal component analysis of gene expression profiles of GFP^{+} tumor cells from WT and *Pfp*$^{-/-}$ *Rag2*$^{-/-}$ mice, non-tumor stromal cells from WT mice, bulk tumors from both mouse types and in vitro cultured cells. All samples were analyzed in triplicate. (**C**) Unsupervised cluster analysis of differentially expressed genes (2-fold cutoff, $P < 0.05$). (**D**) Gene ontology and KEGG pathway analysis of differentially expressed gene clusters (colors correspond to clusters in **C**).

Figure 5

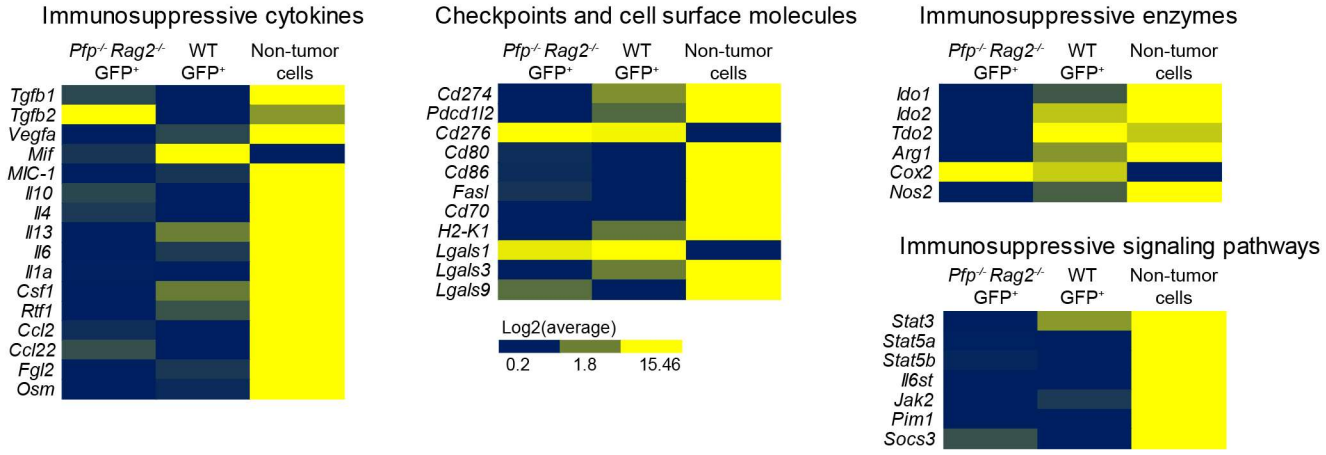

Figure 5: Expression intensity of immunosuppressive genes in tumor cells versus non-tumor cells. Expression levels were determined by RNAseq as shown in Figure 4A.

Figure 6

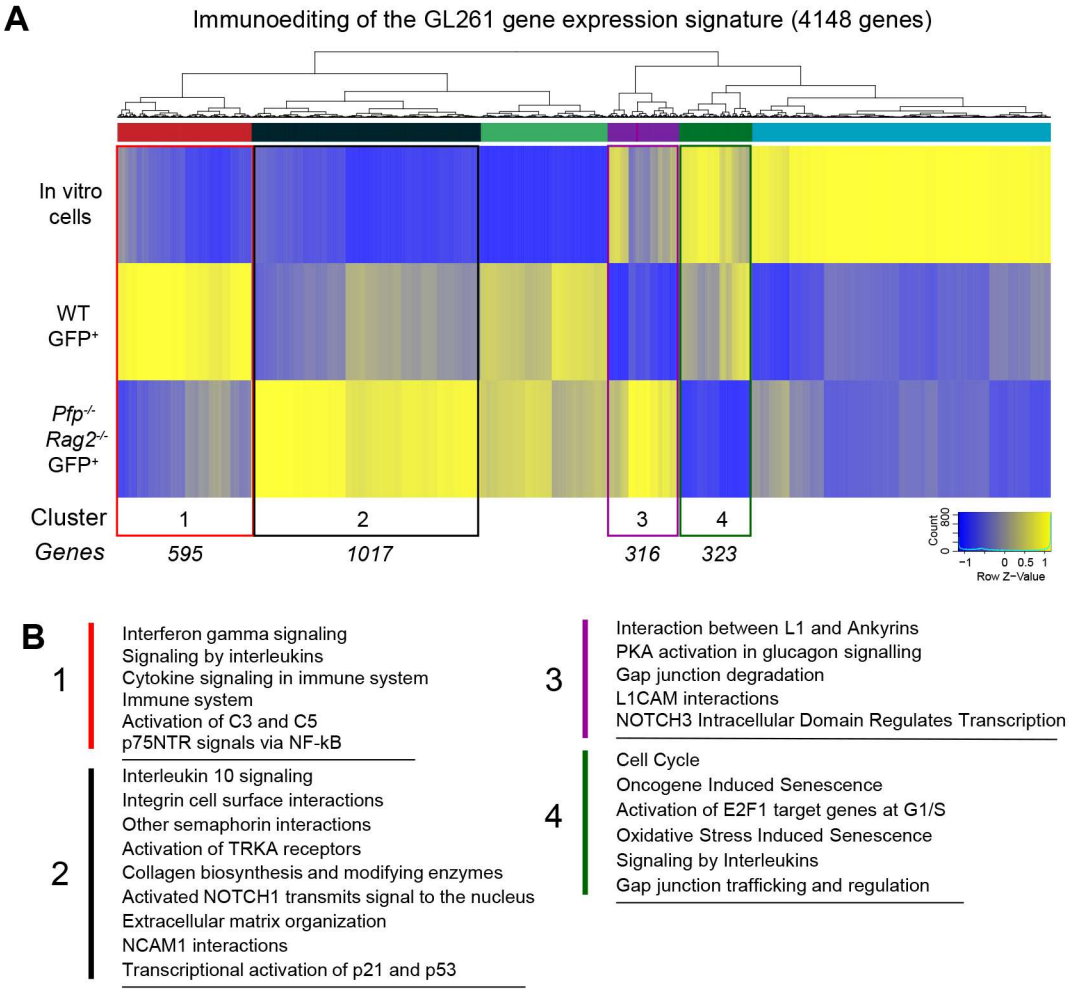

Figure 6: Identification of an immuno-edited tumor cell expression signature. (**A**) Unsupervised hierarchical clustering of differentially expressed genes identify six main clusters, of which four represent genes differentially up- or downregulated in tumors in WT mice versus *Pfp*$^{-/-}$ *Rag2*$^{-/-}$ mice. (**B**) Gene ontology and KEGG pathway analysis of genes upregulated in the four clusters.

Figure 7

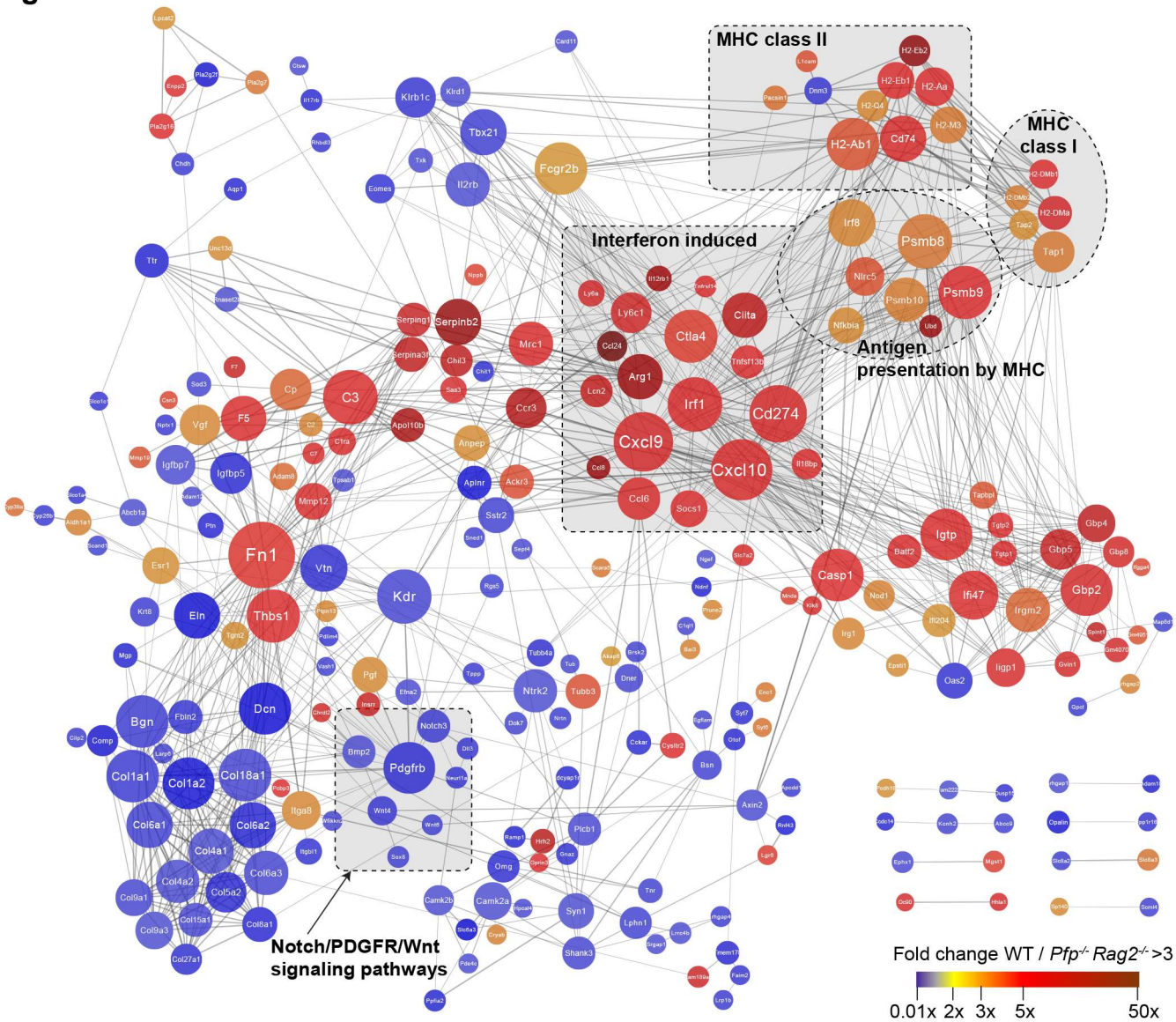

Figure 7
Network analysis of the genes contained in clusters 1-4 (see Figure 6) that are annotated in the STRING database.

Figure 8

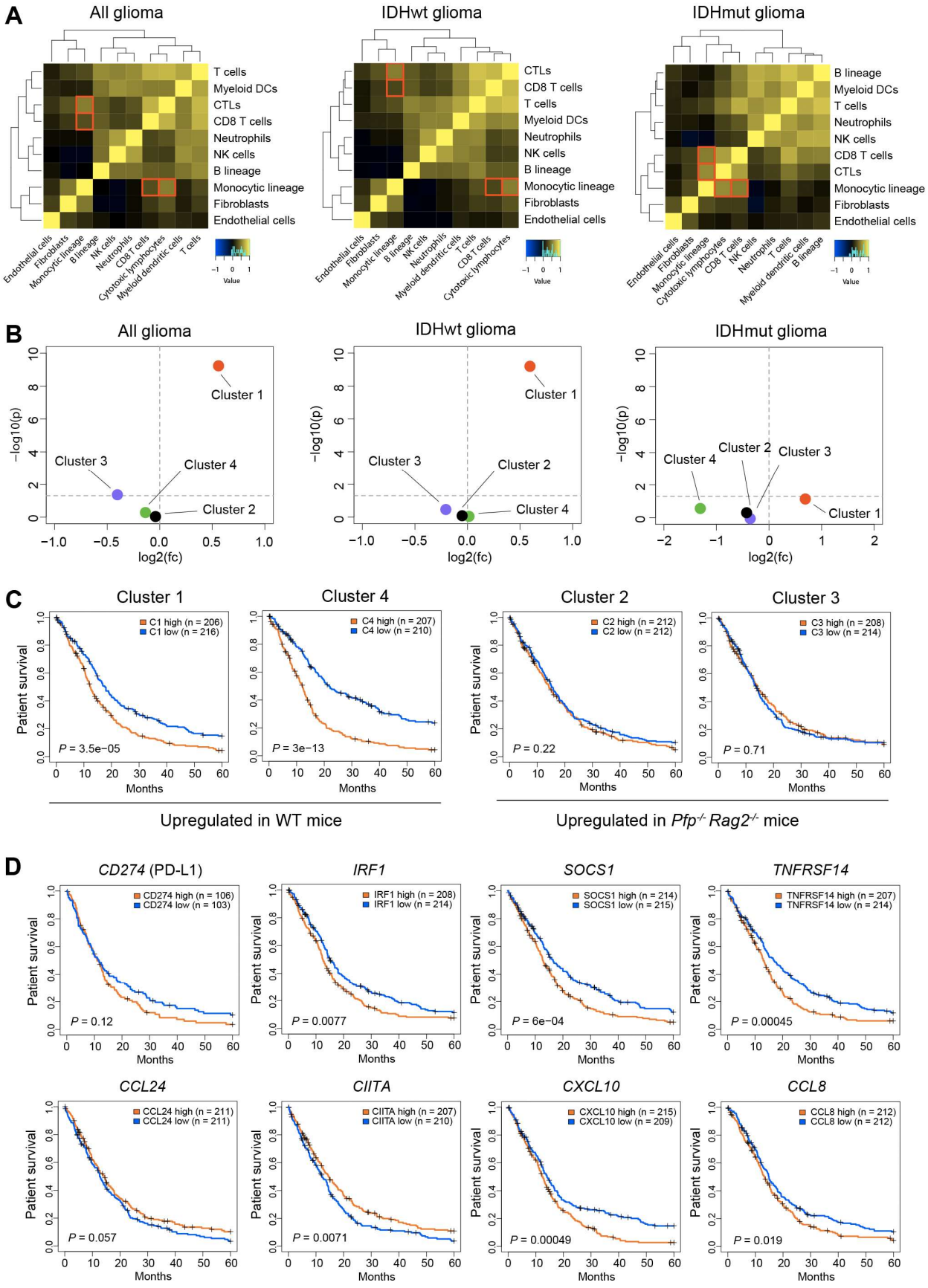

Figure 8: Comparison with human gene expression data.
(**A**) Correlations between different tumor-infiltrating immune and stromal cell subsets in human malignant gliomas. Cytotoxic lymphocytes and CD8$^+$ T cells correlate with monocytic lineage in all gliomas (R = 0.52 and 0.31, respectively, P < 0.001), in particular in IDH-mutated (IDHmut) gliomas (R = 0.52 and 0.57, respectively, P < 0.001). (**B**) Overlap between genes overexpressed in 20% of human gliomas with the highest T-cell gene expression signature (fold-change and P-value, two-sided Fisher test) and the four murine gene clusters identified in Figure 4A. (**C**) Patient survival according to genes over- or under expressed in the 4 murine gene clusters (top versus bottom 20% tumors). (**D**) Kaplan-Meier analysis for individual genes, comparing the 20% of tumors with highest versus lowest expression, log-rank test. See methods for detailed statistics.

Figure 9

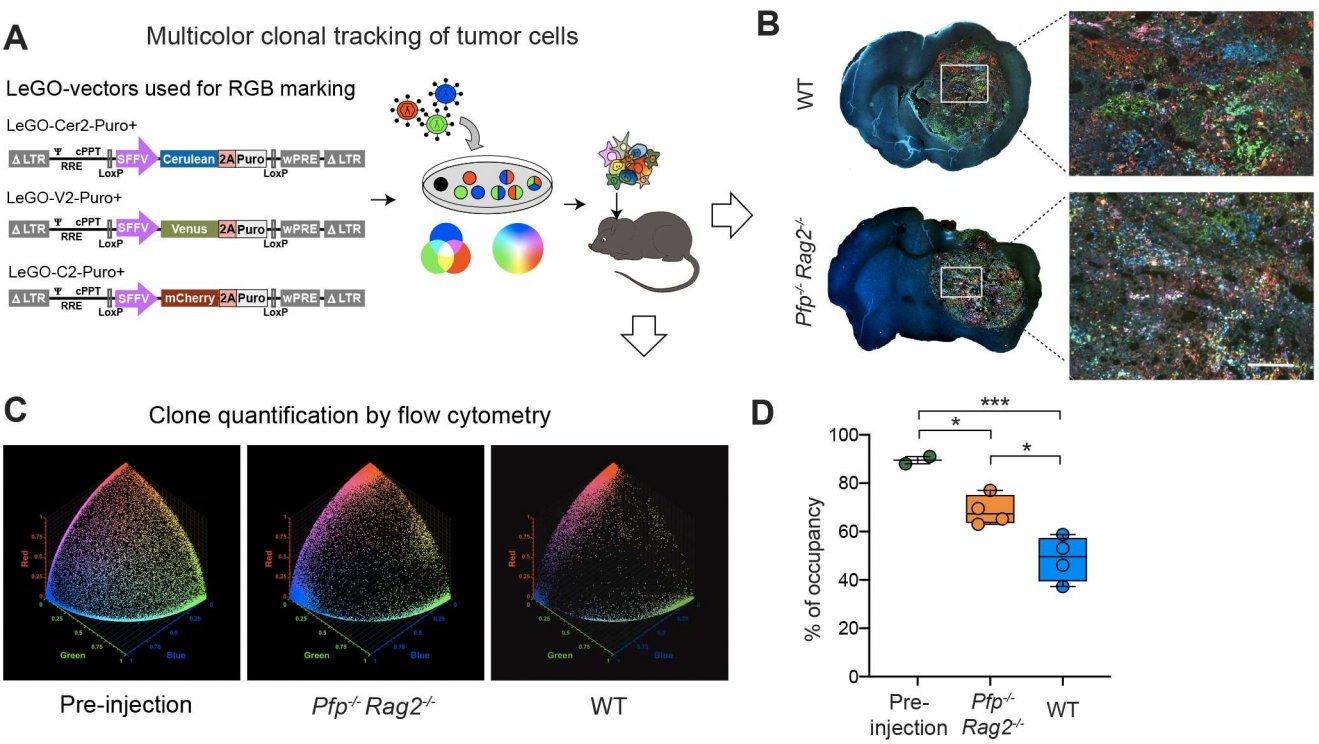

Figure 9: Clonal heterogeneity in RGB-marked tumors.
(**A**) Schematic representation of lentiviral RGB marking of GL261 cells. Fluorescent proteins of the three basic colors are mixed at different but highly stable expression intensities so that all perceivable colors are generated. (**B**) Confocal fluorescence microscopy of RGB-marked GL261 tumors in WT and *Pfp*$^{-/-}$ *Rag2*$^{-/-}$ mice. Scale bar represents 50 µm. (**C**) Spherical scatter plot of cells analyzed by flow cytometry. Each data point designates the chromaticity value of a cell. Note the reduced occupancy, i.e. the plot area occupied with data points in WT mice compared to *Pfp*$^{-/-}$ *Rag2*$^{-/-}$ mice and to the pre-injection mix. (**D**) Quantification of occupancy after multistep dimensionality reduction validates significantly higher clonal contraction in tumors in WT mice than in *Pfp*$^{-/-}$ *Rag2*$^{-/-}$ mice, compared to the multiclonal pre-injection mix. Box plots with IQR (box), mean (line) and max/min (whiskers). One-way ANOVA (P = 0.001) with Tukey's post-hoc test (*P < 0.05, ***P = 0.001); n = 4 per mouse group, n = 2 for the pre-injection mix).

Figure 10

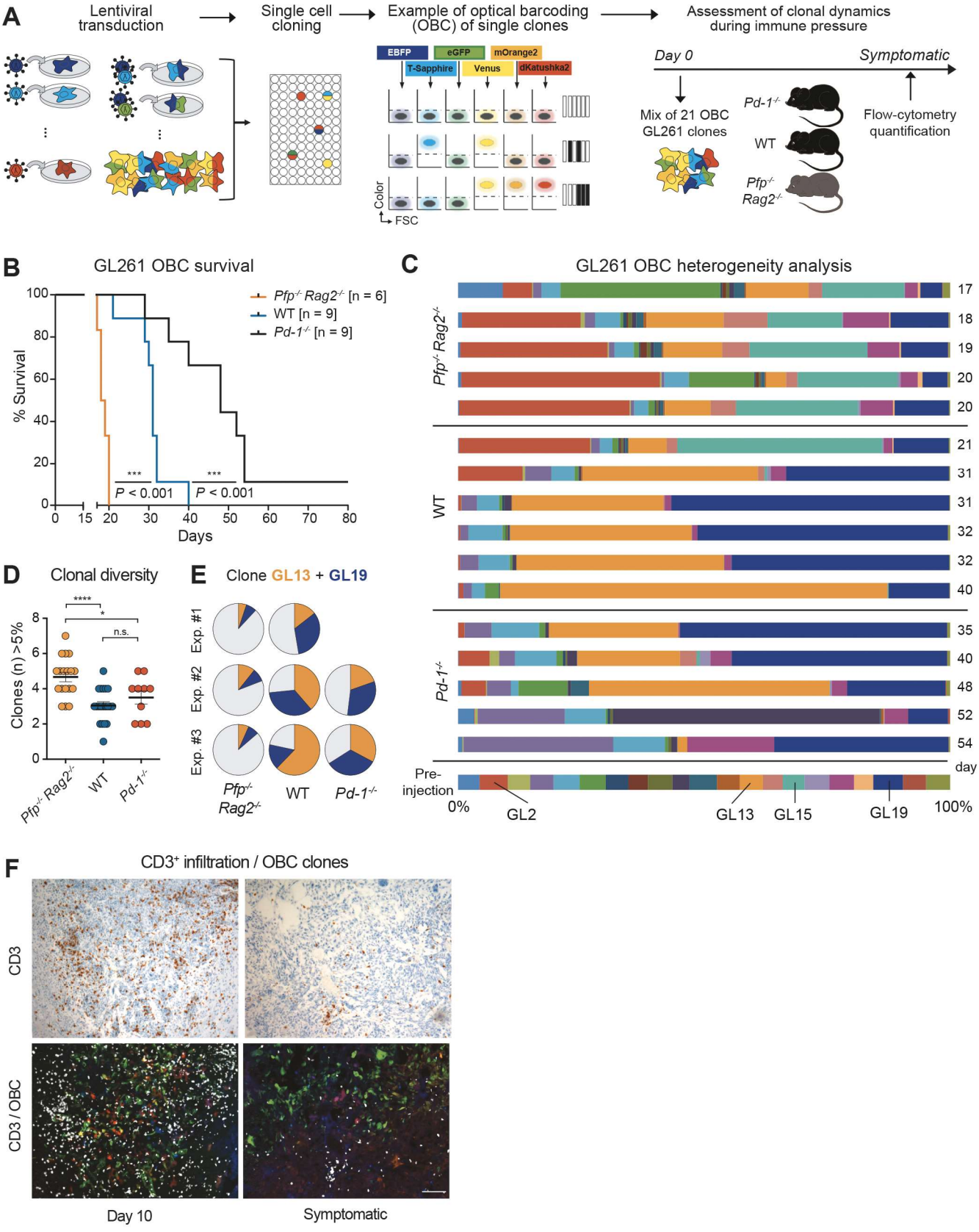

Figure 10: Clonal composition in OBC-marked tumors.
(**A**) Workflow of GL261 optical barcoding and analysis of tumors in mice. (**B**) Survival of mice implanted with OBC-labeled GL261 cells, Kaplan-Meier analysis, log-rank test. (**C**) Flow cytometry analysis of the clonal tumor composition in mice that became symptomatic at the indicated timepoints (days). (**D**) Number of clones that contribute more than 5% to the total number of tumor cells. One-way ANOVA ($P = 0.0001$) with Tukey's post-hoc test (*$P < 0.05$, ****$P < 0.0001$; n.s., not significant; *Pfp*$^{-/-}$ *Rag2*$^{-/-}$ $n = 18$, WT $n = 20$, *Pd-1*$^{-/-}$ $n = 10$). (**E**) Mean dominance of clones GL13 and GL19 in repeat experiments. (**F**) Tumor infiltration with CD3^{+} T cells is maximal on day 10 and parallels the progressive loss of clonal heterogeneity in WT mice. Scale bar represents 100 µm.